Hyperon and Antihyperon Production in $\bar{p}$-p Collisions at 7 BeV/c*†

C. Y. CHIEN,‡ J. LACH, J. SANDWEISS, H. D. TAFT, AND N. YEH§

Physics Department, Yale University, New Haven, Connecticut

AND

Y. OREN‖ AND M. WEBSTER

Brookhaven National Laboratory, Upton, New York

(Received 6 July 1966)

Production of hyperons and antihyperons in the interactions of 6.935 BeV/c antiprotons with protons has been studied. A total of 80 000 pictures taken with the Brookhaven National Laboratory 80-in. liquid-hydrogen bubble chamber have been analyzed for all possible final states involving the production of a hyperon and/or an antihyperon. The total cross section for events in this category is 1.3±0.1 mb. Reactions leading to two-, three-, or four-body final states involving Λ or Σ hyperons (or their antiparticles) were produced highly peripherally. The angular distribution of the ΛΛ̄ final state can be fitted to K^* (888) exchange when the absorptive effect of competing channels is taken into account. Ratios among cross sections of various hyperon-antihyperon pair states agree with predictions from SU_3 symmetry, assuming a dominant K or K^* exchange and an F-type coupling. Charge ratios of events with $\Sigma^\pm$ and $Y_1^{*\pm}$ (1385) are also consistent with single-particle-exchange models. We have examined the mass spectra of all possible mass combinations of all possible final states. The Y_1^* (1385) was by far the most prominent resonance produced, and production of Y_0^* (1405) and Y_0^* (1520) was also observed. Although the energy available in the production center-of-mass system is 3.86 BeV, there was no statistically significant evidence for the production of any new meson or baryon resonance. A thorough search has been made for Ω^- and $\bar{\Omega}^+$ particles, but no event was found to be consistent with their production and decay.

I. INTRODUCTION

WE report here the data on the production of hyperons and antihyperons in the interactions of 7-BeV/c antiprotons with protons.[1–16] A total anti-

proton path length of 0.54×10^6 m in liquid hydrogen has been examined for all events involving the production of a hyperon and/or an antihyperon. The purpose of this experiment was to study the properties of all strangeness -1, -2, and -3 hyperons and their antiparticles; to study the production mechanism in the processes in which these particles were produced; and to obtain the cross sections for these processes.

Hyperon and antihyperon production has been studied previously at lower energies by several groups.[2] Figure 1 shows the energy dependence of some relevant

[1] Some of the preliminary results at 7 BeV/c have been previously reported (Ref. 3–7).

[2] Aside from this experiment, production of hyperons and/or antihyperons in $\bar{p}$-p collisions has been studied by several groups at the following antiproton beam momenta: 1.6, 2.7, 3.0, 3.3, 3.6, 3.7, 4.0, and 5.7 BeV/c (Ref. 8–14).

[3] This sample of film has also been studied for elastic scattering and pion production (Ref. 15) and annihilations into kaons (Ref. 16).

[4] C. Baltay, C. Y. Chien, T. Ferbel, H. L. Kraybill, J. Lach, J. Sandweiss, H. D. Taft, N. Yeh, D. J. Crennell, J. K. Kopp, Y. Oren, D. L. Stonehill, A. M. Thorndike, and M. Webster, in *Proceedings of the 12th Annual International Conference on High Energy Physics at Dubna 1964* (Atomizdat, Moscow, 1965).

[5] C. Baltay, C. Y. Chien, J. Lach, J. Sandweis, P. Slattery, H. D. Taft, J. K. Kopp, Y. Oren, A. M. Thorndike, and M. Webster, in *Proceedings of the 12th Annual International Conference on High Energy Physics at Dubna, 1964* (Atomizdat, Moscow, 1965), p. 693.

[6] C. Baltay, C. Y. Chien, J. Lach, J. Sandweiss, H. D. Taft, Y. Oren, A. M. Thorndike, and M. S. Webster, Bull. Am. Phys. Soc. 10, 65 (1965).

[7] Chih-Yung Chien, Doctoral thesis, Yale University, 1966 (unpublished).

[8] J. Button, P. Eberhard, G. R. Kalbfleisch, J. E. Lannutti, G. R. Lynch, B. Maglić, M. L. Stevenson, and N. Xuong, Phys. Rev. 121, 395 (1961).

[9] W. J. Kernan, D. E. Bohnig, L. S. Schroeder, V. Domingo, A. Eide, G. Fisher, R. Sears, and J. VonKrogh, Bull. Am. Phys. Soc. 11, 360 (1966).

[10] B. Musgrave, G. Petmezas, L. Riddiford, R. Böck, E. Fett,
B. R. French, J. B. Kinson, C. Peyrou, M. Szeptycka, J. Badier, M. Badier, M. Bazin, L. Blaskovic, B. Equer, S. R. Bornestein, S. J. Goldsack, P. E. Grieve, D. H. Miller, J. Meyer, D. Revel, B. Tallini, and S. Zylberajch, in *Proceedings of the Siena International Conference on Elementary Particles and High Energy Physics*, edited by G. Bernardini and G. P. Puppi (Societa Italiana di Fisica, Bologna, 1963), Vol. I, p. 301.

[11] B. Musgrave, G. Petmezas, L. Riddiford, R. Böck, E. Fett, B. R. French, J. B. Kinson, C. Peyrou, M. Szeptycka, J. Badier, M. Bazin, B. Equer, J. Huck, S. Borenstein, S. J. Goldsack, D. H. Miller, S. Misbahuddin, J. Meyer, D. Revel, B. Tallini, and S. Zylberajch, in *Proceedings of the Siena International Conference on Elementary Particles and High Energy Physics*, edited by G. Bernardini and G. P. Puppi (Societa Italiana di Fisica, Bologna, 1963), Vol. I, p. 312.

[12] Data at both 3.25 and 3.7 BeV/c had been reported in many places; they had been summarized in a recent article with references given to all previous reports. See C. Baltay, J. Sandweiss, H. D. Taft, C. B. Culwick, J. K. Kopp, R. I. Louttit, R. P. Shutt, A. M. Thorndike, and M. S. Webster, Phys. Rev. 140, B1027 (1965).

[13] R. Böck, A. Cooper, B. R. French, R. Levi-Setti, D. Revel, B. Tallini, and S. Zylberajch, in *Proceedings of the 12th Annual International Conference on High Energy Physics at Dubna, 1964* (Atomizdat, Moscow, 1965), p. 686.

[14] R. K. Böck, W. A. Cooper, B. R. French, J. B. Kinson, R. Levi-Setti, D. Revel, B. Tallini, and S. Zylberajch, Phys. Letters 17, 166 (1965).

[15] J. A. Johnson, Doctoral thesis, Yale University, 1965 (unpublished).

[16] N. Kuei-Eng Yeh, Doctoral thesis, Yale University, 1966 (unpublished).
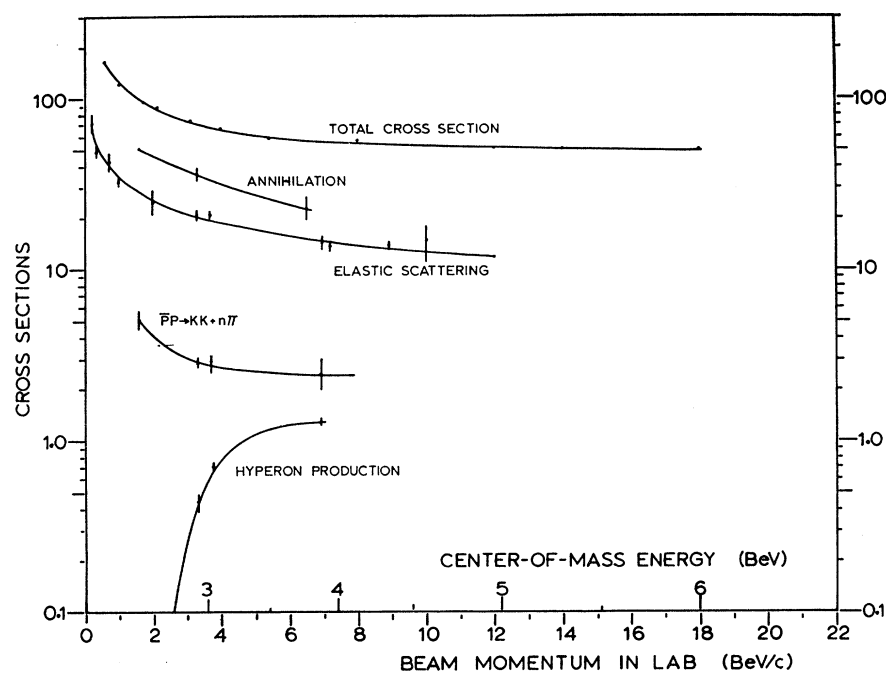
FIG. 1. $\bar{p}$-p cross sections.

$\bar{p}-p$ cross sections.[17] Less than 2% of all high energy $\bar{p}-p$ interactions involve hyperon and/or antihyperon production. Thus a very large number of $\bar{p}-p$ events are needed to perform any detailed study. However these events are interesting because, in addition to the conventional search for new particles and resonances, they also supply knowledge of the properties of anti-hyperons and their resonant states. Furthermore the two-body hyperon states furnish simple systems for the study of production mechanisms and symmetry properties.

This paper is divided into eight sections: the experimental procedures are explained briefly in Sec. II. (They have been treated in detail in Ref. 7.) In Sec. III we present the cross sections for various final states and a comparison with data at lower energy. In Sec. IV we report the details of the search for the Ω particle and a

study of the production of Ξ particles. Lifetimes and masses of some hyperons and antihyperons are reported in Sec. V. The two-body final states are of particular interest since they furnish very simple systems to study interaction mechanisms. They are treated in detail in Sec. VI with a comparison with some theoretical predictions from single-particle exchange models and SU_3 symmetry. Data on three- and four-body final states also have some bearing on the single particle exchange models; they are presented in Sec. VII. Finally Sec. VIII summarizes this experiment.

II. EXPERIMENTAL PROCEDURES

A. The Exposure

The antiprotons were produced by the 28-BeV/c internal proton beam of the Brookhaven National Laboratory Alternating Gradient Synchroton (AGS) impinging on an aluminum target in the AGS I-10 straight section. The particles were then taken off at 7° from the primary beam and traversed a complex of magnets and separators known as Beam 3,[18] finally entering the BNL 80 in. liquid-hydrogen bubble chamber.[19]

[17] The data used in Fig. 1 were collected from Ref. 8, 12, 15, 16, and the following reports: T. Ferbel, A. Firestone, J. Johnson, H. Kraybill, and J. Sandweiss, Nuovo Cimento 38, 12 (1965); 38, 19 (1965); U. Amaldi, T. Fazzini, G. Fidecaro, C. Ghesquiere, M. Legros, and H. Steiner, *ibid.* 34, 825 (1964); W. Galbraith, E. W. Jenkins, T. F. Kycia, B. A. Leontic, R. H. Phillips, A. L. Read, and R. Rubenstein, Phys. Rev. 138, B913 (1965); Charles A. Coombes, Bruce Cork, William Galbraith, Glen R. Lamberston, and William Wenzel, *ibid.* 112, 1303 (1958); T. Elioff, L. Agnew, O. Chamberlain, H. Steiner, C. Wiegand, and T. Ypsilantis, Phys. Rev. Letters 3, 285 (1959); Rafael Armenteros, Charles A. Coombes, Bruce Cork, Glen R. Lamberston, and W. A. Wenzel, Phys. Rev. 119, 2068 (1960); T. Ferbel, A. Firestone, J. Sandweiss, H. D. Taft, M. Gailloud, T. W. Morris, A. H. Bachman, P. Baumel, and R. M. Lea, *ibid.* 137, B1250 (1965); H. C. Dehne, E. Raubold, P. Söding, M. W. Teucher, G. Walf, and E. Lohrman, Phys. Letters 9, 185 (1964); K. J. Foley, S. J. Lindenbaum, W. A. Love, S. Ozaki, J. J. Russell, and L. C. Yuan, Phys. Rev. Letters 11, 503 (1963); and G. Kalbfleisch, University of California Radiation Laboratory Report UCRL-9597 (unpublished).

[18] I. Skillicorn and M. Webster, Brookhaven National Laboratory Internal Report H-10, 1962 (unpublished); D. C. Rahm, Brookhaven National Laboratory Internal Report H-17, 1965 (unpublished).

[19] J. G. Androulakis, J. A. Bamberger, D. P. Brown, H. O. Courtney, B. B. Culwick, J. J. Diener, W. B. Fowler, C. L. Goodzeit, J. Hanush, E. L. Hart, H. Houtsager, J. E. Jensen, D. A. Kassner, D. T. Liverios, R. I. Louttit, S. C. No, T. W. Morris, R. B. Palmer, P. A. Pion, R. R. Rau, E. Rutan, R. P. Shutt, J. H. Sondericker, A. M. Thorndike, W. A. Tuttle, I. J. Winters, W. Woelfel, D. H. Wright, S. S. Yamamoto, F. Anderson, H. W. Courant, and H. L. Kraybill, Nucl. Inst. Methods 20, 100 (1963).

FIG. 2. Schematic layout of beam 3.

Fiducials: A (-25.347, +19.079, 0)
            D (+55.877, -19.098, 0)

Cameras: 1 (-31.75 , -31.75 , -207.49)
           2 (+31.75 , -31.75 , -207.49)
           3 (+31.75 ; +31.75 , -207.49)
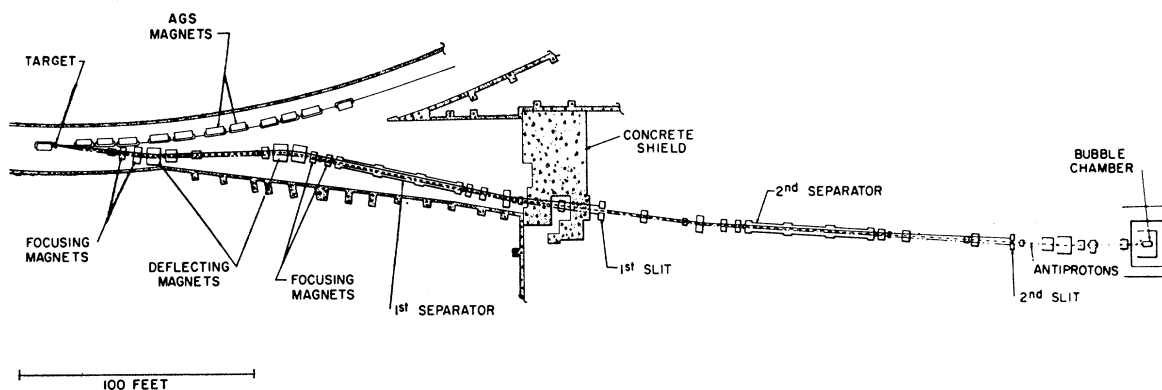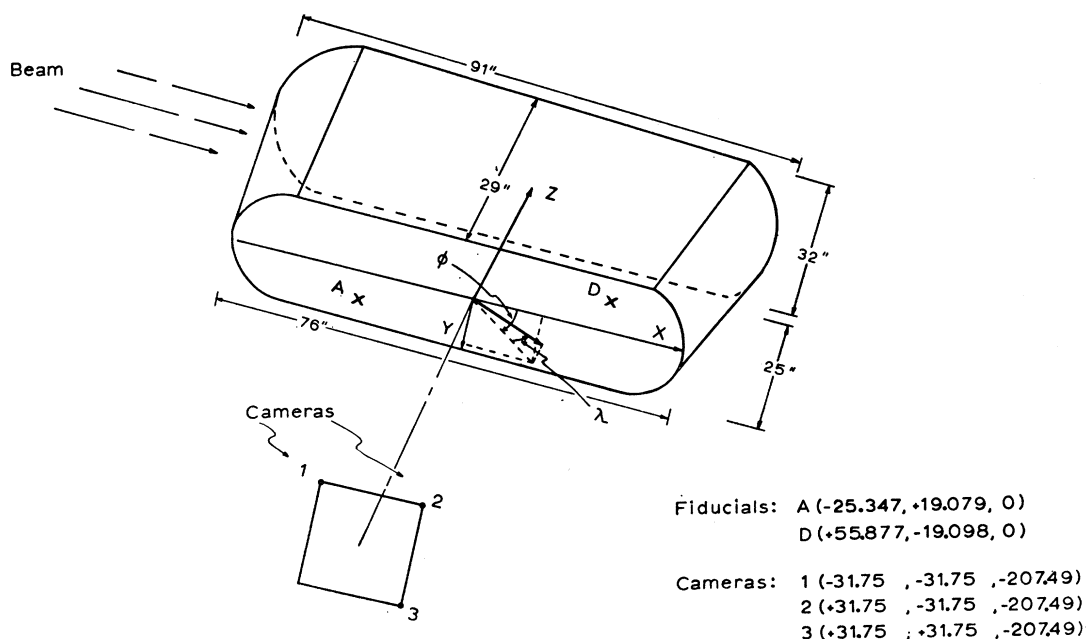
FIG. 3. Dimensions of the BNL 80-in. liquid-hydrogen bubble chamber, YACK coordinate system, and the positions of fiducials and cameras. Fiducial and camera coordinates are in cm.

The over-all length of Beam 3 from the I-10 target to the 80-in. bubble chamber was approximately 450 ft. It was a two-stage electrostatically separated beam with a 50 ft long separator in each stage (Fig. 2).

Figure 3 shows schematically the dimensions of the BNL 80-in. bubble chamber, the positions of the fiducials used and the three cameras, and the coordinate system used in this study. The magnetic field had a large Z component of approximately 20 kG which varied by as much as ±3 kG over the hydrogen volume. It also had X and Y components of from -2 to $+2$ kG. All three components had been accurately measured and fitted to polynomials of the X, Y, and Z coordinates in space and thus could be calculated for any point in the chamber.[20]

[20] B. B. Culwick, Brookhaven National Laboratory Internal Report B.C. 05-2-G, 1964 (unpublished).

A total of 80 000 pictures were taken in February 1964 with an average of 10 antiprotons per frame. The effective length of the chamber was reduced to approximately 50 in. due to the dislocation of some of the retrodirective "coat hangers" near the beginning of the chamber. Chamber parameters were adjusted during the run to obtain bubble diameters of about 350 μ and a bubble density of about 10 bubbles per cm for tracks of minimum ionization. This made possible estimation of particle velocities for tracks with ionization up to three times minimum.

The purity of the beam was determined to be 95% from a careful study of the momentum spectrum of δ rays produced by beam-like tracks.[15] The beam momentum was determined from elastic $\bar{p}$-p scatterings.[15] In these events the momentum of the outgoing proton was accurately determined from the range-energy rela-

tions in liquid hydrogen. The measured momenta of the incoming and outgoing $\bar{p}$ were ignored and a 2-constraint fit was performed. This procedure gave an accurate value for the beam momentum for each event. The resulting momentum distribution had a width of $\pm 1\%$ (at half-maximum) and a central value of 6.935 BeV/c. However, the event analysis was carried out with an assumed beam momentum spread of $\pm 2\%$. We have determined that the event identification was unaffected by the use of this larger beam spread. For brevity we will refer to the beam momentum as 7 BeV/c.

B. Scanning

The film was divided evenly between Yale and BNL and was processed separately until all events had been scanned, measured and identified.

The scanning was done using conventional scanning machines. The BNL film was scanned twice, once for Ω events, and once for events with either two or more visible strange particle decays or events with a zero-prong and a vee. The latter is referred to as the "double decay" scan. The Yale film had two total strange particle scans, i.e., scans for events with at least one strange particle decay, in addition to the Ω scan and "double decay" scan. Scanning efficiencies were determined after events from all scans had been measured, fitted and identified. The over-all scanning efficiency for the Yale sample was determined to be 98%. The efficiency for the BNL sample was estimated to be 87% for events with kinks and 75% for events with only vees.

A count of the number of beam-like particles was also made on every tenth frame in each scan. This gave a total beam count of 4.23×10^5 antiprotons in the Yale sample and 4.40×10^5 antiprotons in the BNL sample. There was approximately one hyperon event in every 40 pictures.

C. Measuring

After the film had been scanned events from the BNL sample were measured with conventional manual measuring machines. Yale events were measured by two digitized measuring machines monitored by a Digital Equipment Corporation PDP-1 Comupter.[21] The PDP-1 used in this system had a memory of 16 000 18-bit words, a paper tape reader-punch, a typewriter, and a magnetic tape unit. After a track was measured, the PDP-1 checked for logical mistakes and then reconstructed the track in three dimensions. An error message was relayed to the measurer via a typewriter and a closed-circuit television system if the track failed any of the logical checks or reconstruction criteria. The track was then immediately remeasured. Before any event in a frame was completed, the PDP-1 checked the association of every vee with each possibly associated vertex by calculating the coplanarity and transverse momentum balance. It also checked the nature

of each vee by calculating and checking the effective mass of the vee interpreted as an electron pair, K_1^0 decay, Λ decay, and $\bar{\Lambda}$ decay. The measurer completed the measurement of a frame only after the nature and association of all vees in that frame had been determined. The PDP-1 wrote the completed measurement of an event onto an output magnetic tape only after the whole event had passed logical and reconstruction checks. These features enabled us to obtain a 95% pure sample of well measured events with associated strange particle decays. This resulted in great savings in measuring, film handling, analysis, and bookkeeping efforts.

D. Kinematic Fitting and Event Identification

Measurements from both laboratories were processed with YACK—the Yale reconstruction and fitting program. YACK is an IBM 7094 computer program which first reconstructs every track and calculates its momentum and space angles in three dimensions and then fits the events to different final state interpretations.

A total of 3379 strange-particle events were measured and fitted to all kinematically possible and fittable final states with two or three strange particles.[22] Most of these events fitted more than one final state. Ambiguities were then reduced by applying χ^2 cutoffs, visual ionization estimates, and in some cases, missing mass cutoffs (Secs. VI-A and VII-B). After this process, 1868 events were identified as hyperon events (with hyperon and/or antihyperon production), 1296 events[16] were identified as annihilations into kaons and pions, while the rest of the events were ambiguous between these two categories. Among these 1868 hyperon events, 604 events had unique fits while the rest of them had ambiguous fits or fits with more than one missing neutral. Chi-square distributions, angular distributions, mass spectra, etc. were computed separately for both the Yale and BNL events. Since no substantial differences were noted in these distributions the events were merged and subsequent analysis was done on the combined sample. All of these events were used for cross-section calculations while the unique events supplied most of the other data presented in this paper.

III. CROSS SECTIONS

Approximately one half of the hyperon events were not detected in the bubble chamber because the strange particles produced were not visible for one or more of the following reasons: (1) They decayed into all neutral products. (2) They decayed too close to the production vertex to be detected or they decayed outside the visible

---

[21] H. Taft and P. Martin (unpublished).

[22] All events with two prongs and two vees or with four prongs and one vee have been fitted to all kinematically possible final states including those with four strange particles such as $\Lambda\bar{\Lambda}K\bar{K}+n\pi$. However, among 260 events in these two types, only two events made any of these four-strange-particle fits, and these two events were ambiguous with some two-strange-particle final states. Thereafter any final states involving four strange particles were not attempted in our kinematic fitting programs.

TABLE I. Hyperon-antihyperon production cross sections.[a]

Final states	Number of unique events observed	σ (μb)
$\Lambda\bar{\Lambda}$	62	40±6
$\Lambda\bar{\Sigma}^0$	38	39±6
$\Sigma^{\pm}\bar{\Sigma}^{\mp}$	15	19±9
$\Sigma^+\bar{\Lambda}\pi^-$	90	105±18
$\Sigma^-\bar{\Lambda}\pi^+$	33	35±8
$\Sigma^+\bar{\Sigma}^0\pi^-$	1	5±5
$\Sigma^-\bar{\Sigma}^0\pi^+$	1	2±2
$\Lambda\bar{\Lambda}\pi^+\pi^-$	59	59±12
$\Lambda\bar{\Sigma}^0\pi^+\pi^-$	19	9±5
$\Sigma^{\pm}\bar{\Sigma}^{\mp}\pi^+\pi^-$	14	12±5
$\Sigma^+\bar{\Lambda}\pi^+\pi^-\pi^-$	16	24±8
$\Sigma^-\bar{\Lambda}\pi^+\pi^+\pi^-$	15	12±4
$\Lambda\bar{\Lambda}\pi^+\pi^+\pi^-\pi^-$	12	8±4
$^{\Lambda}_{\Sigma^0}\bar{\Lambda}+m\pi^0,\ m\geqslant 1$	109	158±21
$^{\Lambda}_{\Sigma^0}\bar{\Sigma}^-\pi^++m\pi^0,\ m\geqslant 1$	69	52±11
$^{\Lambda}_{\Sigma^0}\bar{\Sigma}^+\pi^-+m\pi^0,\ m\geqslant 1$	43	34±5
$^{\Lambda}_{\Sigma^0}\bar{\Lambda}\pi^+\pi^-+m\pi^0,\ m\geqslant 1$	112	77±9
$\Sigma^{\pm}\bar{\Sigma}^{\mp}\pi^+\pi^-+m\pi^0,\ m\geqslant 1$	8	14±6
$^{\Lambda}_{\Sigma^0}\bar{\Lambda}\pi^+\pi^+\pi^-\pi^-+m\pi^0,\ m\geqslant 1$	12	9±4

[a] The following notations are used: (1) Each cross section given is for the state listed and its charge conjugate. (2) Y stands for Λ, Σ^+, Σ^0, or Σ^-, and $\bar{Y}$ stands for $\bar{\Lambda}$, $\bar{\Sigma}^+$, $\bar{\Sigma}^0$, or $\bar{\Sigma}^-$.

TABLE II. Associated production cross sections.[a]

Final states	Number of unique events observed	σ (μb)
$\Lambda K^0\bar{n}$	34	69±17
$\Lambda K^+\bar{p}$	47	71±14
$\Sigma^0 K^+\bar{p}$	21	51±13
$\Sigma^+ K^0\bar{p}$	9	15±8
$\Lambda K^0\bar{p}\pi^+$	42	46±14
$\Sigma^0 K^0\bar{p}\pi^+$	11	7±5
$\Lambda K^0\bar{n}\pi^+\pi^-$	4	6±3
$\Lambda K^+\bar{p}\pi^+\pi^-$	12	8±3
$\Lambda K\bar{N}3\pi$	6	4±2
$^{\Lambda}_{\Sigma^0}K^0\bar{n}+m\pi^0,\ m\geqslant 1$	45	87±22
$^{\Lambda}_{\Sigma^0}K^+\bar{p}+m\pi^0,\ m\geqslant 1$	39	106±53
$\Sigma^+ K^0\bar{p}+m\pi^0,\ m\geqslant 1$	8	19±8
$\Sigma^{\pm}K^0\bar{n}\pi^{\mp}+l\pi^0,\ l\geqslant 0$	34	67±14
$^{\Lambda}_{\Sigma^0}K^0\bar{p}\pi^++m\pi^0,\ m\geqslant 1$	25	23±9
$^{\Lambda}_{\Sigma^0}K^0\bar{n}\pi^+\pi^-+m\pi^0,\ m\geqslant 1$	3	13±8
$^{\Lambda}_{\Sigma^0}K^+\bar{p}\pi^+\pi^-+m\pi^0,\ m\geqslant 1$	15	8±3

[a] The following notations are used: (1) Each cross section given is for the state listed and its charge conjugate. (2) Y stands for Λ, Σ^+, Σ^0, or Σ^-, and $\bar{Y}$ stands for $\bar{\Lambda}$, $\bar{\Sigma}^+$, $\bar{\Sigma}^0$, or $\bar{\Sigma}^-$.

chamber volume. (3) The charged strange particles had projected decay angles on the film too small to be detected. In order to correct for these losses, a fiducial volume was designated by using minimum and maximum limits on the coordinates of both production and decay vertices. Minimum limits were also imposed on the strange-particle track length and projected charged-particle decay angle. This fiducial volume was determined to give a reliable and unbiased scanning efficiency and acceptable measurements. Only events inside this volume were used to calculate cross sections. They were weighted by a Monte Carlo program. For each strange particle event with its strange particles decaying inside the fiducial volume, this program generated 500 fake events using the momenta and space angles of that event and averaging over all the parameters with known distributions such as the position of the reactions in the chamber, and the rotation of the event around the incident beam direction.[23] All decay products were assumed to be isotropically distributed in the c.m. of the decaying particle. The detection efficiency for that event was then the ratio of the number of fake events inside the fiducial volume to the total number of fake events

generated. The weight W_i of the event was defined as the reciprocal of the detection efficiency of the entire event. The total number of events of a certain kind was then calculated to be

$$N = (1/e)[\sum_i W_i \pm (\sum_i W_i^2)^{1/2}],$$

where e is the scanning efficiency.

Criteria were also established to define a beam track. Events with beam tracks failing to satisfy these criteria were also rejected in cross-section calculations. The average effective path length of accepted beam tracks was

$$l = 87.96\ \text{cm},$$

which was the potential path length of a beam track inside the fiducial volume averaged over the geometrical beam distribution and corrected for the attenuation of antiprotons in hydrogen assuming a total $\bar{p}$-p cross section of 59 mb.[15] The total effective antiproton path length in hydrogen was then

$$L = 0.54 \times 10^6\ \text{m},$$

which was the product of the average effective path length and the total count of beam tracks satisfying the beam criteria corrected by the beam purity factor.

The total cross section was then calculated using all hyperon events. Tables I and II give the cross sections of each final state and they are summarized in Table III with a comparison with data at 3.7 BeV/c.[12] This

[23] The mass, lifetime, and decay branching ratio of each particle used in this program were taken from the article of A. H. Rosenfeld, A. Barbaro-Galtieri, W. H. Barkas, P. L. Bastien, J. Kirz, and Matts Roos, Rev. Mod. Phys. 36, 977 (1964).

TABLE III. Hyperon production cross sections—summary.[a]

Final states	σ (μb) at 7 BeV/c	σ (μb) at 3.7 BeV/c
$Y\bar{Y}$	98 ± 12	203 ± 16
$Y\bar{Y}\pi$	162 ± 20	
$Y\bar{Y}+2\pi$	80 ± 14	378 ± 30
$Y\bar{Y}+j\pi,\ j\geqslant3$	367 ± 32	
$YK\bar{N}$	206 ± 27	101 ± 25
$YK\bar{N}+m\pi,\ m\geqslant1$	384 ± 39	9 ± 3
Ξ production	14 ± 5	5
Ω production	$\leqslant3$	$\cdots$
Total	1310 ± 105	720 ± 30

[a] The following notations are used: (1) Each cross section given is for the state listed and its charge conjugate. (2) Y stands for Λ, Σ^{+}, Σ^{0}, or Σ^{-}, and $\bar{Y}$ stands for $\bar{\Lambda}$, $\bar{\Sigma}^{+}$, $\bar{\Sigma}^{0}$, or $\bar{\Sigma}^{-}$.

table shows that the increase in total cross section is due to the great increase in the cross sections for associated production and production of hyperon-antihyperon pairs with additional pions.

IV. STUDY OF Ω AND Ξ PRODUCTION

A. Search for the Ω Particle

It has been pointed out that the baryon resonances $N^{*}(1238)$, $Y_{1}^{*}(1385)$, and $\Xi^{*}(1532)$ can be arranged as a SU_{3} decuplet with one member still missing.[24–26] The tenth member, named Ω^{-} by Gell-Mann, should have quantum numbers

$$B=1,\quad Q=-1,\quad T=0,\quad S=-3,\quad J^{P}=\tfrac{3}{2}+.$$

Its mass was further predicted by the Gell-Mann–Okubo mass formula as approximately 1680 MeV.[27] The existence of the Ω^{-} particle has been considered to be a crucial test of the theory of unitary symmetry of strong interactions since the 10-dimensional representation of the SU_{3} symmetry group can be identified with just this decuplet.

A thorough search for the Ω^{-} and its antiparticle has been carried out in this experiment.[4] No event has been found which could be interpreted as the production and decay of the Ω^{-} hyperon or its antiparticle, although the existence of the Ω^{-} has been reported in several high-energy $K^{-}p$ experiments.[28–30]

[24] M. Gell-Mann, in *Proceedings of the 1962 Annual International Conference on High Energy Physics* at CERN, edited by J. Prentki (CERN, Geneva, 1962), p. 805.
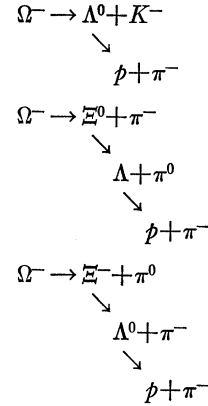
[25] S. L. Glashow and J. S. Sakurai, Nuovo Cimento **25**, 337 (1962).

[26] J. Behrends, J. Dreitlein, C. Fronsdal, and W. Lee, Rev. Mod. Phys. **34**, 1 (1962).

[27] S. Okubo, Prog. Theoret. Phys. (Kyoto) **27**, 949 (1962); M. Gell-Mann, Synchrotron Laboratory, California Institute of Technology Internal Report CTSL-20, 1961 (unpublished).

[28] V. E. Barnes, P. L. Connolly, D. J. Crennell, B. B. Culwick, W. C. Delaney, W. B. Fowler, P. E. Hagerty, E. L. Hart, N. Horwitz, P. V. C. Hough, J. E. Jensen, J. K. Kopp, K. W. Lai, J. Keitner, J. L. Lloyd, G. W. London, T. W. Morris, Y. Oren, R. B. Palmer, A. G. Prodell, D. Radojicic, D. C. Rahm, C. R. Richardson, N. P. Samios, J. R. Sanford, R. P. Shutt, J. R. Smith,

Events with at least one kink and an associated vee, or with two consecutive kinks on the same track with or without additional vees, were scanned for and measured. They were then fitted to the following chains of decays:

$$\Omega^{-}\rightarrow\Lambda^{0}+K^{-}$$
$$\searrow$$
$$p+\pi^{-}$$

$$\Omega^{-}\rightarrow\Xi^{0}+\pi^{-}$$
$$\searrow$$
$$\Lambda+\pi^{0}$$
$$\searrow$$
$$p+\pi^{-}$$

$$\Omega^{-}\rightarrow\Xi^{-}+\pi^{0}$$
$$\searrow$$
$$\Lambda^{0}+\pi^{-}$$
$$\searrow$$
$$p+\pi^{-}$$

and their charge conjugates. The mass of the Ω in these fits was allowed to vary between 1670 and 1690 MeV.[30] In addition to these interpretations fits were also attempted for the Ξ, Σ, and K interpretations of the decaying tracks.

Among a total of 209 candidates, only two made fits to one of the above Ω decay modes, but their fits were inconsistent with the observed bubble density of the tracks, and they were both identified as Ξ^{-} decays. All the other 207 events had reasonable alternative fits consistent with the observed bubble densities.

The detection efficiency of this search is a function of the product of the momentum and mean lifetime assumed for the Ω. The momentum of the Ω in the laboratory system was kinematically limited to be between 1.5 and 5.5 BeV/c in this experiment. Assuming the most favorable Ω lifetime for its detection, $\approx2\times10^{-10}$ sec[30], the upper limit of Ω^{-} and/or $\bar{\Omega}^{+}$ production in this experiment is 3 μb. This upper limit is insensitive to the exact Ω momentum for the assumed Ω^{-} lifetime.

B. Ξ Production

Eleven Ξ^{-} or $\bar{\Xi}^{+}$ particles were observed in this experiment and decayed as

$$\Xi^{-}\rightarrow\pi^{-}+\Lambda^{0}$$
$$\searrow$$
$$p+\pi^{-}$$
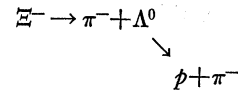
D. L. Stonehill, R. C. Strand, A. M. Thorndike, M. S. Webster, W. J. Willis, and S. S. Yamamoto, Phys. Rev. Letters **12**, 204 (1964).

[29] G. S. Abrams, R. A. Burnstein, G. R. Charlton, T. B. Day, B. Kehoe, B. Sechi-Zorn, G. A. Snow, M. C. Whatley, G. Wolsky, G. B. Yodh, and R. G. Glasser, Phys. Rev. Letters **13**, 670 (1964).

[30] So far seven Ω^{-} decays have been observed in several $K^{-}p$ experiments. Their averaged mass and lifetime are

$$m=1674.5\pm4.4\ \text{MeV},$$
$$\tau=(1.9\pm0.7)\times10^{-10}\ \text{sec}.$$

See N. P. Samios, Proceedings of the Argonne International Conference on Weak Interactions, 1965, p. 210 (to be published).

or its charge conjugate, where both the Ξ and the Λ decays were visible. These decays were uniquely identified because they were either 4- or 3-constraint fits, depending on the Ξ track length. The cross section for the production of Ξ^- and/or $\bar{\Xi}^+$ was determined to be

$$\sigma = 14 \pm 5 \ \mu b.$$

The 11 Ξ^- and $\bar{\Xi}^+$ particles were produced in 10 events. Three of these events have pairs of Ξ and $\bar{\Xi}$ with one or more pions; the other seven events have $\Xi \bar{\Lambda}(\bar{\Sigma}^0) K$ or their charge conjugates with or without pions.

The angular distribution of the Ξ^- and $\bar{\Xi}^+$ (Fig. 4) in the $\bar{p}$-p center-of-mass system is very different from those of other baryons and antibaryons observed in this study. Figure 4 shows an isotropic distribution rather than the usual forward-backward peaking observed in all other two-, three-, and four-body final states (Secs. VI and VII). This is not very surprising since these events can not be produced by the exchange of any known particle. On the other hand, a study of all the Λ and $\bar{\Lambda}$ particles observed in this experiment shows that, while the majority of them were produced peripherally, about 10% of them were also produced isotropically in the $\bar{p}$-p center-of-mass system (Fig. 5).

V. OBSERVATION OF HYPERONS AND ANTIHYPERONS

All the presently known strangeness -1 hyperons Λ, Σ^0, Σ^+, Σ^- and their antiparticles have been observed in this experiment as well as Ξ^- and $\bar{\Xi}^+$. The neutral Ξ particles were not studied because their decay fits were usually ambiguous with other decay hypotheses.

Masses of some of these particles were calculated by using a maximum likelihood method and the observed Gaussian distributions for their masses. The best value for the mass and its error were thereby calculated from

$$m^* = \frac{\sum_i m_i/(\Delta m_i)^2}{\sum_i 1/(\Delta m_i)^2}, \quad \Delta m^* = [\sum_i (\Delta m_i)^{-2}]^{-1/2},$$

where m_i and Δm_i are the effective mass and its error of a hyperon calculated from its decay products.

A maximum likelihood method was used to obtain the lifetimes of various hyperons and antihyperons.
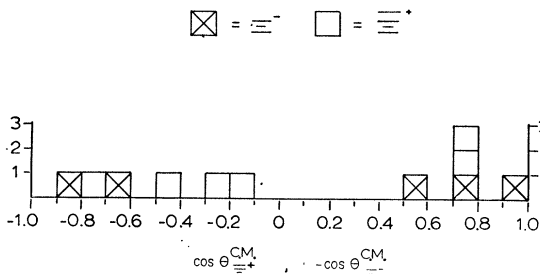
$$\boxtimes \ = \ \Xi^- \qquad \square \ = \ \bar{\Xi}^+$$

FIG. 4. Angular distribution of $\bar{\Xi}^+$ and Ξ^- (folded observed in the $\bar{p}$-p center-of-mass system.
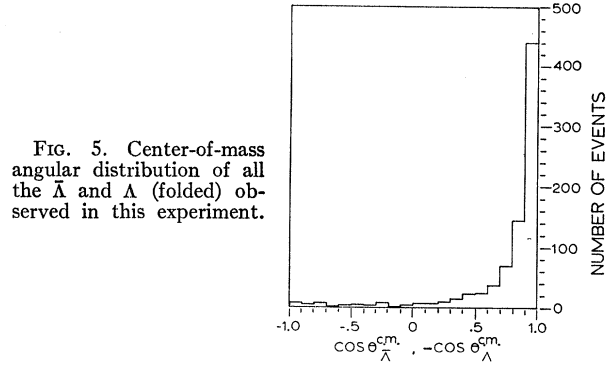
FIG. 5. Center-of-mass angular distribution of all the $\bar{\Lambda}$ and Λ (folded) observed in this experiment.

The likelihood function was defined as

$$L(\tau) = \prod_i \tau^{-1} \exp(-t_i/\tau)$$

$$\times [\exp(-t_i^{min}/\tau) - \exp(-t_i^{max}/\tau)]^{-1},$$

where τ is the assumed lifetime of the particle (proper time), t_i is the observed lifetime (proper time), t_i^{min} is the minimum proper-time cutoff in the observation due to the minimum track-length cutoff (0.5 cm), and t_i^{max} is the maximum proper time cutoff in the observation due to the fiducial volume.

Table IV shows the number of events and the results of mass and of lifetime calculations. In these calculations, variables from decay fits were used in all cases. For $\Sigma^\pm$ and $\bar{\Sigma}^\pm$ calculations the only events used were from $\pi^\mp \Sigma^\pm \bar{\Lambda}$, $\bar{p}\Sigma^+ K^0$, and $\Sigma^\pm \bar{\Lambda}\pi^\mp \pi^+ \pi^-$ final states and their charge conjugates where fits were usually very reliable (4- or 3-constraint) and there were no ambiguities between $\Sigma^\pm$ and $\bar{\Sigma}^\pm$.

Errors quoted in Table IV are purely statistical. We estimated that the systematic errors in lifetime calculations are small compared with the quoted statistical errors. The systematic errors in mass calculations are about 0.10 MeV. However, we believe that the systematic errors should be the same for both particles and antiparticles. Therefore the mass difference between Λ and $\bar{\Lambda}$ is 0.05±0.06 MeV and that between Ξ^- and $\bar{\Xi}^+$ is 1.0±1.1 MeV. It is clear from Table IV that the masses and lifetimes of the antiparticles are consistent with being equal to those of their corresponding particles, as required by CPT invariance.

TABLE IV. Hyperon masses and lifetimes[a]

Particle	Mass (MeV)	Lifetime (10^{-10} sec)	Number of decays used
Λ	1115.74±0.04	2.50±0.14	1147
$\bar{\Lambda}$	1115.69±0.05	2.70±0.20	972
Σ^+		0.86±0.15	125
$\bar{\Sigma}^-$		1.10±0.24	117
Σ^-		2.08±0.22	61
$\bar{\Sigma}^+$		1.46±0.31	64
Ξ^-	1321.67±0.52	1.37±0.51	6
$\bar{\Xi}^+$	1320.69±0.93	1.51±0.55	5

[a] Errors quoted are purely statistical. The systematic errors in the mass calculations are estimated to be about 0.1 MeV.
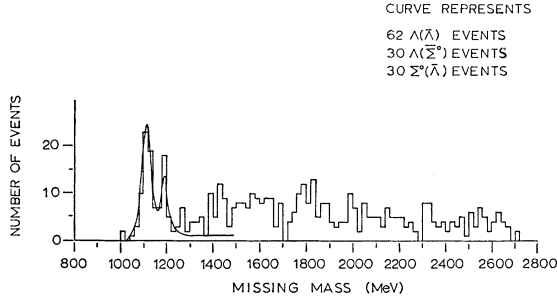
CURVE REPRESENTS

62 Λ(Λ̄) EVENTS
30 Λ(Σ̄⁰) EVENTS
30 Σ⁰(Λ̄) EVENTS

FIG. 6. Missing mass of the neutrals in $\bar{p}+p \to \Lambda+$neutrals; both single-vee and double-vee events are included.

VI. TWO-BODY FINAL STATES

A. Neutral Two-Body Final States

The possible neutral two-body hyperon final states in this experiment were

$$\bar{p}+p \to \Lambda+\bar{\Lambda} \tag{1}$$

$$\bar{p}+p \to \Lambda+\bar{\Sigma}^0 \tag{2}$$

$$\bar{p}+p \to \Sigma^0+\bar{\Lambda} \tag{3}$$

$$\bar{p}+p \to \Sigma^0+\bar{\Sigma}^0 \tag{4}$$

$$\bar{p}+p \to \Xi^0+\bar{\Xi}^0. \tag{5}$$

The last two reactions were not treated in our kinematic fitting program. Because the Σ^0 and the $\bar{\Sigma}^0$ have very short lifetimes (probably $<10^{-14}$ sec), the first four reactions all appeared in the bubble chamber as a Λ decay and/or an $\bar{\Lambda}$ decay associated with a disappearing incoming $\bar{p}$ beam track. When both Λ and $\bar{\Lambda}$ decays are visible they can usually be identified kinematically as one of reactions (1–3), or one of these with additional missing neutral pions. However, of the events with only one decay visible, 80% were ambiguous between two or more of the above interpretations. Figure 6 shows the missing mass distribution of all zero-pronged events with at least a visible Λ decay, i.e., the mass of all the neutral particles produced with the Λ. There are two well separated peaks at the $\bar{\Lambda}$ and the $\bar{\Sigma}^0$ masses which correspond to events of reactions (1) and (2). An attempt was subsequently made to separate these events according to their missing masses. The corresponding distribution for events with a visible $\bar{\Lambda}$ shows that the resolution was too poor to resolve the Λ and Σ^0 peaks. Those events were therefore not used in further studies.

The expected missing-mass distributions of events in reactions (1) and (2) are two resolution functions centered at the $\bar{\Lambda}$ and the $\bar{\Sigma}^0$ masses, respectively. Those for reactions (3) and (4) where the observed Λ came from the decay of Σ^0 are two nearly uniform spectra spreading from 1125 to 1650 MeV and from 1200 to 1700 MeV, respectively. Events with missing mass lower than 1260 MeV in Fig. 6 were therefore fitted to a mixture of the above reactions by a maximum-likelihood method. Reactions (2) and (3) were assumed to have the same rate in this fit since they are charge

conjugate states and the Λ detection efficiency is practically the same in both reactions. The best fit obtained is shown by the solid curve in Fig. 6. We thereafter designated the events with missing mass less than 1160 MeV as $\Lambda\bar{\Lambda}$ events and those with missing mass between 1160 and 1240 MeV as $\Lambda\bar{\Sigma}^0$ events. Their differential cross sections are shown in Figs. 7(a) and 7(b). According to the best fit in Fig. 6, we estimated that there was a contamination of 8% $\Lambda\bar{\Sigma}^0$ or $\Sigma^0\bar{\Lambda}$ in the $\Lambda\bar{\Lambda}$ sample; and 7% $\Lambda\bar{\Lambda}$, 16% $\Sigma^0\bar{\Lambda}$, and 1% $\Sigma^0\bar{\Sigma}^0$ in the $\Lambda\bar{\Sigma}^0$ sample. However, the background of $\Lambda\bar{\Sigma}^0$ and $\Sigma^0\bar{\Lambda}$ events in the $\Lambda\bar{\Lambda}$ angular distributions is not serious because the background is very small, and the distribution of the background events is very similar to that of the real events. For the same reason, the background of $\Lambda\bar{\Lambda}$ events in the $\Lambda\bar{\Sigma}^0$ distribution is not serious either. For those $\Sigma^0\bar{\Lambda}$ events which were interpreted as $\bar{\Lambda}\Sigma^0$ events, the production angle obtained from the incorrect fits are in general not the true production angles. At the present energy, however, the error thus introduced in $\cos\theta_{c.m.}$ is generally very small ($\leqslant 0.026$). For these reasons, Figs. 7(a) and 7(b) can be considered as distributions of pure $\Lambda\bar{\Lambda}$ and pure $\Lambda\bar{\Sigma}^0$ events. These distributions are not weighted. However weighting does not change their shapes since these events have nearly uniform weights.

Figs. 7(a) and 7(b) show that the hyperons (Λ) are sharply backward peaked. (The forward direction, $\cos\theta_{c.m.}=1$, in the production center-of-mass system was defined as the direction of the incoming antiproton in this study.) In other words, the hyperons tend to keep the direction of the target protons whereas the
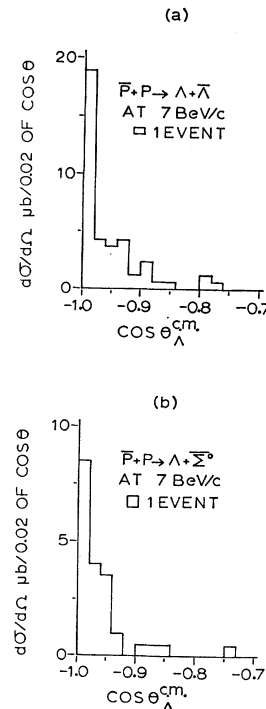
(a)

$\bar{P}+P \to \Lambda+\bar{\Lambda}$
AT 7 BeV/c
□ 1 EVENT

(b)

$\bar{P}+P \to \Lambda+\bar{\Sigma}^0$
AT 7 BeV/c
□ 1 EVENT

FIG. 7. (a) Angular distribution of Λ in $\bar{p}+p \to \Lambda+\bar{\Lambda}$ in the $\bar{p}$-p center-of-mass system normalized to total $\Lambda\bar{\Lambda}$ cross section. (b) Angular distribution of Λ in $\bar{p}+p \to \Lambda+\bar{\Sigma}^0$ in the $\bar{p}+p$ center-of-mass system normalized to total $\Lambda\bar{\Sigma}^0$ cross section.

TABLE V. $\bar{p}+p \to \bar{Y}+Y$ cross sections (in μb) compared with the octet exchange model of SU_3.[a]

Beam momentum BeV/c		$\Lambda\bar{\Lambda}$[b]	$\Lambda\bar{\Sigma}^0+\Sigma^0\bar{\Lambda}$	$\Sigma^0\bar{\Sigma}^0$ [c]	$\Sigma^+\bar{\Sigma}^-$	$\Sigma^-\bar{\Sigma}^+$
3.0	σ	117±18	102 ±17	<18	31 ±5	9.5±4
	ratio	9± 1.4	7.8± 1.3	<1.4	2.4± 0.4	0.73
3.25	σ	87±13	56 ±11	<19	36 ±13	2^{+8}_{-2}
	ratio	9± 1.3	5.8± 1.1	<2	3.7± 1	0.21
3.6	σ	77±20	67 ±19	<22	23 ±6	11 ±4.5
	ratio	9± 2.3	7.8± 2	<2.5	2.6±0.7	1.3±0.5
3.7	σ	82± 8	69 ±10	<26	44 ±9	8 ±4
	ratio	9± 0.9	7.6± 1	<2.8	4.8±1	0.9±0.4
4.5	σ	39±16	46 ±13	<17	$18.5^{+6}_{-3.5}$	$8^{+3}_{-4.5}$
	ratio	9± 3.7	10.6± 3	<4	4.3±1.2	1.8±1
6.9	σ	40± 6	39 ± 6	<9	16 ±9	3 ±2
	ratio	9± 1.7	8.8± 1.6	<2.0	4 ±2	0.6
$8a(F)$[a]		9	6	1	4	...
$8s(D)$[a]		1	6	9	36	...

[a] K. Tanaka, Phys. Rev. **135**, B1186 (1964).
[b] The $\Lambda\bar{\Lambda}$ cross section was normalized to 9 in the calculation of experimental ratios.
[c] Deduced from charge independence using $\Sigma^+\bar{\Sigma}^-$ and $\Sigma^-\bar{\Sigma}^+$.

antihyperons tend to keep the direction of incoming antiprotons in the production center-of-mass system. This forward-backward peaking has also been reported at lower energies, but it has become more pronounced at this higher energy. These remarkably peripheral angular distributions strongly suggest that these events were produced through some exchange mechanism and the exchanged particle must be a singly charged meson with a strangeness of 1. Therefore it must be a K, K^*, or any system of a kaon and pions. Many theoretical attempts have been made to explain the sharpness of this forward-backward peaking.[31–39] Some good fits to the angular distributions at various energies have been achieved when a strong dominance of $K^*(888)$ exchange is assumed and when the absorptive effect of competing channels is taken into account.[36–39] However, the energy dependence of the cross sections of these channels is not correctly described in this model. For instance the cross section in this experiment is about $\frac{1}{2}$ of the value predicted by this model if the $NK^*\bar{\Lambda}$ coupling constant determined by lower energy data is used.[38,39]

B. $\Sigma^+\bar{\Sigma}^-$ and $\Sigma^-\bar{\Sigma}^+$ Final States

Events with charged sigma pairs appeared in the bubble chamber as a beam track with two charged

prongs where one or both prongs displayed a kink. These events presented some experimental difficulties because the presence of the neutral decay product reduced the Σ decay fit to a 1-constraint fit, and because the decaying tracks were often so short as to further reduce the fit to 0 constraint. This happened very often because the hyperons were usually very slow in the laboratory system as they were produced backward in the $\bar{p}$-p center-of-mass system. Due to these difficulties, events with only one kink were very ambiguous and therefore were not used in this study. Those events with both kinks visible could be uniquely identified as $\Sigma^+\bar{\Sigma}^-$ from X^2 or ionization analysis if one or both charged decay products happened to be a proton or antiproton. Otherwise they were usually ambiguous between $\Sigma^+\bar{\Sigma}^-$ or $\Sigma^-\bar{\Sigma}^+$ because the mass difference between Σ^+ and Σ^- is only 8 MeV.

Fifteen events were identified as charged Σ pair production in this experiment. From consideration of the Σ^+ decay branching ratio and the detection efficiencies of Σ^+ and Σ^- decays, the data are consistent with 13 $\Sigma^+\bar{\Sigma}^-$ and 2 $\Sigma^-\bar{\Sigma}^+$ events. Their angular distribution in the $\bar{p}$-p center-of-mass system is shown in Fig. 8. It is consistent with all antihyperons being produced in the forward direction in the $\bar{p}$-p center-of-mass (c.m.) system.
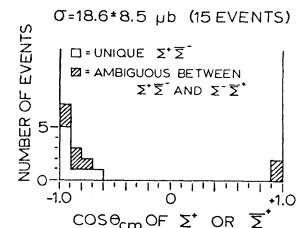
[31] G. C. Summerfield, Nuovo Cimento **23**, 867 (1962).
[32] N. J. Sopkovich, Nuovo Cimento **26**, 186 (1962).
[33] C. H. Chan, Phys. Rev. **133**, B431 (1962).
[34] H. D. D. Watson, Nuovo Cimento **29**, 1338 (1963).
[35] A. Dar, M. Kugler, Y. Dothan, and S. Nussinov, Phys. Rev. Letters **12**, 83 (1964); A. Dar, ibid. **13**, 91 (1964).
[36] Loyal Durand III and Yam Tsi Chiu, Phys. Rev. Letters **12**, 399 (1964); Phys. Rev. **137**, B1530 (1965).
[37] G. Cohen-Tannoudji, and H. Navelet, Nuovo Cimento **37**, 4227 (1965).
[38] H. Högaasen and J. Högaasen, Nuovo Cimento **40**, 8796 (1965).
[39] Yam-Tsi Chiu, Doctoral thesis, Yale University, 1965 (unpublished).

FIG. 8. Center-of-mass angular distribution of Σ^+ or $\bar{\Sigma}^+$ of events identified as $\Sigma^+\bar{\Sigma}^-$ or $\Sigma^-\bar{\Sigma}^+$.
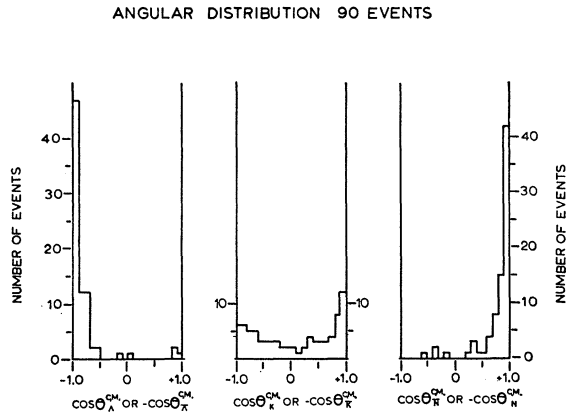
ANGULAR DISTRIBUTION 90 EVENTS

FIG. 9. Angular distributions of events in the $\bar{p}+p \rightarrow \Lambda+K+\bar{N}$ and c.c. final states in the $\bar{p}$-p center-of-mass system.

C. Two-Body Cross Sections Compared with Predictions from SU_3

The highly peripheral angular distributions for the two-body final states discussed in this section strongly suggest the dominance of a K or $K^*(888)$ exchange mechanism. Since both K and K^* are members of an SU_3 octet, this leads to a model for these reactions in which the amplitude associated with the SU_3 octet exchange dominates over amplitudes of other representations connecting $8\otimes 8$ with $8\otimes 8$. There are two independent octet amplitudes: the symmetric octet (D-type coupling) and the antisymmetric octet (F-type coupling). These result in two sets of ratios among various $Y\bar{Y}$ production which were calculated by Tanaka according to this model.[40] Table V shows the theoretical ratios as compared with the results at this

and lower beam momenta. It shows that the experimental results agree reasonably well with the F-type coupling over the entire energy range and sharply disagree with the D-type coupling. It also shows that $\Sigma^-\bar{\Sigma}^+$ production is much smaller than $\Sigma^+\bar{\Sigma}^-$ production, a fact which is consistent with single particle exchange models since the $\Sigma^-\bar{\Sigma}^+$ production requires the exchange of a doubly charged system.

VII. THREE- AND FOUR-BODY FINAL STATES

A. Associated Production

There were 34 events of the type $\Lambda K^0\bar{n}$ or its charge conjugate (c.c.), and 46 $\Lambda K^+\bar{p}$ (or c.c.) events observed in this experiment. These $\Lambda K^+\bar{p}$ (or c.c.) events appeared in the chamber as two prongs with visible Λ (or $\bar{\Lambda}$) decays. They were mostly 4-constraint events with a slow Λ decay or heavily ionizing proton track from the production vertex which made their identification very reliable. A $\Lambda K^0\bar{n}$ (or c.c.) event appeared in the chamber as two visible vees ($K_1{}^0$ and Λ or $\bar{\Lambda}$) associated with a disappearing beam track. They were 1-constraint events since the n (or $\bar{n}$) was missing. Their missing mass distribution shows a clear separation among events with missing n (or $\bar{n}$) and those with both missing n (or $\bar{n}$) and extra neutral pions. These events were therefore separated on the basis of their missing masses.

The angular distribution of these events (Fig. 9) shows that the baryons are sharply peaked backward in the $\bar{p}$-p c.m. system and the antibaryons are sharply peaked forward. This type of forward-backward peaking prevailed in all three-body states and, to a lesser extent, also in four-body states. This suggests that these events were mostly produced by some exchange mechanism
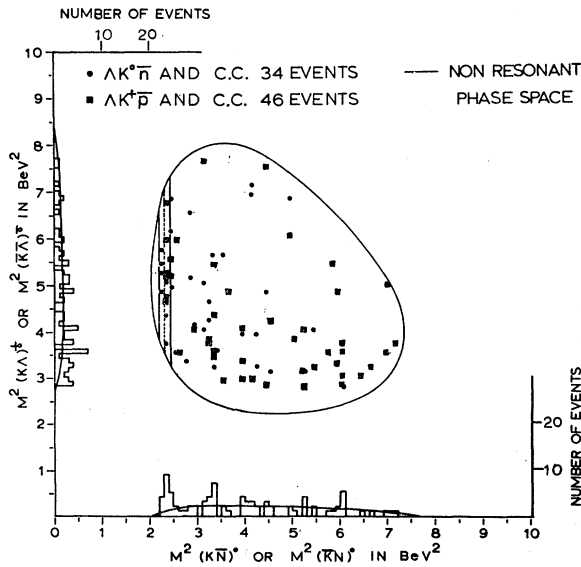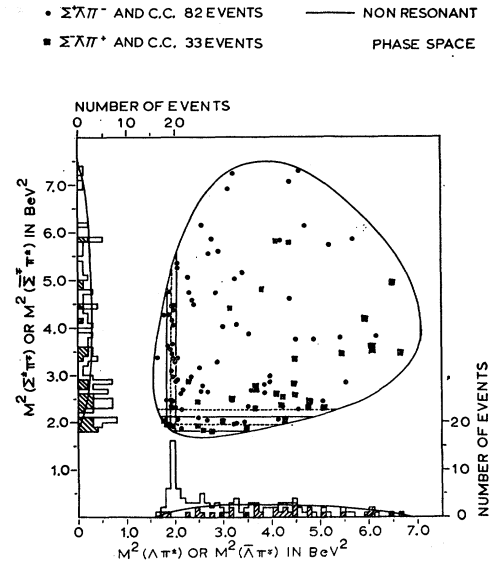

FIG. 10. Dalitz plot of events in the $\bar{p}+p \rightarrow \Lambda+K+\bar{N}$ and c.c. final states. The band corresponds to $Y_0^*(1520)$ ($1505 \leqslant M \leqslant 1535$ MeV).

[40] K. Tanaka, Phys. Rev. **135**, B1186 (1964).

FIG. 11. Dalitz plot of events in the $\bar{p}+p \rightarrow \Sigma^{\pm}\bar{\Lambda}\pi^{\mp}$ and c.c. final states. The band in the $\Sigma\pi$ system corresponds to $Y_0^*(1405)$ ($1350 \leqslant M \leqslant 1460$ MeV), and that in the $\Lambda\pi$ system corresponds to $Y_1^*(1385)$ ($1350 \leqslant M \leqslant 1420$ MeV). The cross-hatched events in the projected histograms are $\Sigma^-\bar{\Lambda}\pi^+$ and c.c. events.

The Dalitz plot (Fig. 10) shows that about 20% of these events proceed through $Y_0^*(1520)$ production.

B. $\Sigma^\pm \overline{\Lambda} \pi^\mp$ and Charge-Conjugate Final States

The final states consisting of $\Sigma^\pm \overline{\Lambda} \pi^\mp$ (or c.c.) are of interest because of their relevance to the single-particle exchange model. If the pion and the lambda were produced at the same vertex, events with Σ^+ or $\overline{\Sigma}^-$ should be favored over those with Σ^- or $\overline{\Sigma}^+$ since the latter involve the exchange of doubly charged systems. On the other hand, if the pion was produced with the Σ in a $T=0$ state, then Σ^+ and Σ^- events should be equally favored.

A total of 115 events was observed in these final states. Of these 82 were events with Σ^+ or $\overline{\Sigma}^-$ as compared with 33 events with Σ^- or $\overline{\Sigma}^+$. The Dalitz plot of these events (Fig. 11) shows strong $Y_1^*(1385)$ production (about 23%), some $Y_0^*(1405)$ production (about 12%), and some indication of $Y_0^*(1520)$ production. The production of these resonances in these final states is not as pronounced as at lower energies (e.g., 40%, 21% and 14%, respectively, at 3.7 BeV/c).[12] However, their cross sections remain approximately the same because the total cross section for these final states is higher at 7 BeV/c. Angular distributions in the $\bar{p}$-p c.m. system are shown in Fig. 12. The forward-backward peaking again suggests that their production is dominated by some exchange mechanism. This is further supported by the fact that in the $Y_1^*(1385)$ band, there are 27 events produced as $\overline{\Sigma}^-Y_1^{*+}(1385)$ (or c.c.) as compared with only one event produced as $\overline{\Sigma}^+Y_1^{*-}(1385)$ (or c.c.). On the other hand, in the $Y_0^*(1405)$ and $Y_0^*(1520)$ regions, Σ^+ and Σ^- are equally produced. The pion distribution in Fig. 12 is also interesting. The open events in the forward and backward directions correspond to $\pi^-\overline{\Lambda}\Sigma^+$ (and c.c.) events produced peripherally with $Y_1^*(1385)$ and Y_0^*, respectively. The cross-hatched events in the forward direction correspond to $\pi^+\overline{\Lambda}\Sigma^-$ (and c.c.) events produced peripherally with Y_0^*. These are all consistent with single-particle exchange models.
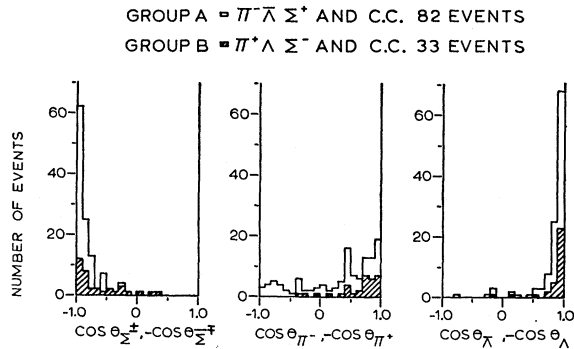
GROUP A = $\pi^-\overline{\Lambda}$ Σ^+ AND C.C. 82 EVENTS

GROUP B = $\pi^+\Lambda$ Σ^- AND C.C. 33 EVENTS

FIG. 12. Center-of-mass angular distributions of events in the $\bar{p}+p \to \pi^\mp\overline{\Lambda}\Sigma^\pm$ and c.c. final states. The cross-hatched events are $\overline{\Sigma}^-\overline{\Lambda}\pi^+$ and c.c. events.
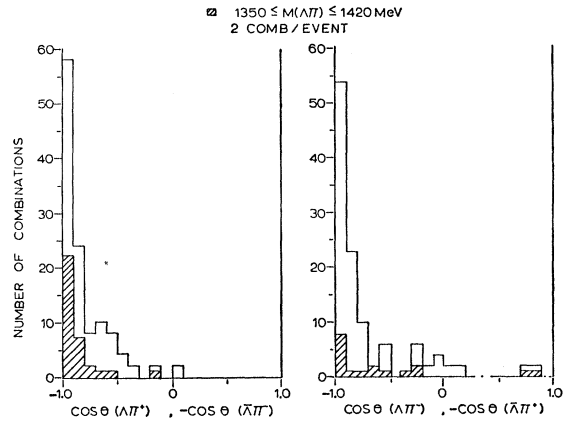
FIG. 13. Center-of-mass angular distributions of $\Lambda\pi^+$ (and folded $\overline{\Lambda}\pi^-$) and $\Lambda\pi^-$ (and folded $\overline{\Lambda}\pi^+$) in the $\bar{p}+p \to \Lambda+\overline{\Lambda}+\pi^+$ $+\pi^-$ final states. Cross-hatched combinations are those with their mass in $Y_1^*(1385)$ region, i.e., $1350 \leqslant M(\Lambda\pi) \leqslant 1420$ MeV.

C. The $\Lambda\overline{\Lambda}\pi^+\pi^-$ Final State

These events appeared in the bubble chamber as two prongs with a Λ and/or a $\overline{\Lambda}$ decay visible. Forty-one of these events had both vees visible and therefore made very reliable 4-constraint fits. Those events in which only the Λ or $\overline{\Lambda}$ decayed visibly were often ambiguous with the $\Lambda K^+\pi^-\bar{n}$ (or c.c.) final state because one of the two prongs was ambiguous between a pion and a kaon. In these single-vee events only the unique events were used. The mass spectra and angular distribution of these events were compared with those of the double-vee events. No significant differences were found indicating that excluding ambiguous single-vee events did not introduce any serious bias.
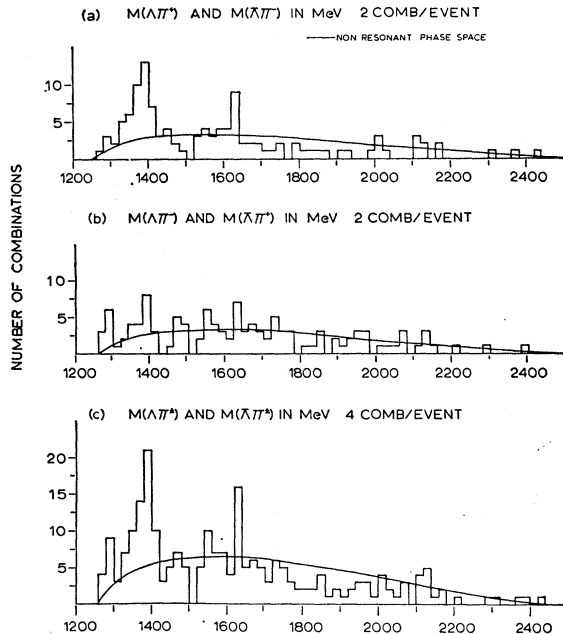
FIG. 14. Histograms of the effective masses of the $\Lambda\pi$ systems in 59 events in $\bar{p}+p \to \Lambda+\overline{\Lambda}+\pi^++\pi^-$ final states.
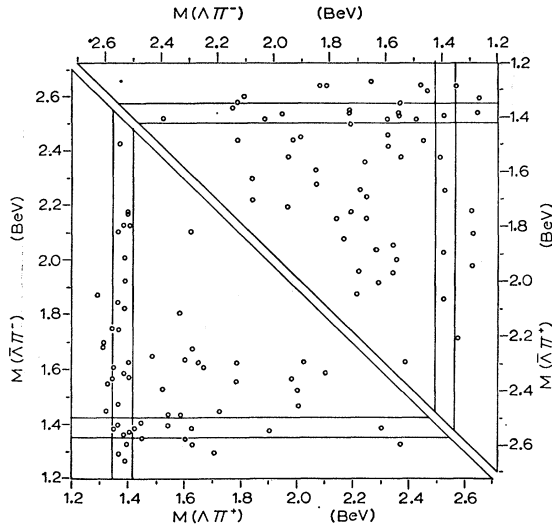
M($\Lambda\pi^-$)   (BeV)

M($\bar{\Lambda}\pi^-$) (BeV)

M($\bar{\Lambda}\pi^+$)

M($\Lambda\pi^+$)   (BeV)

FIG. 15. Scattergrams of $M(\bar{\Lambda}\pi^+)$ versus $M(\Lambda\pi^-)$ (top) and $M(\bar{\Lambda}\pi^-)$ versus $M(\Lambda\pi^+)$ (bottom) of 59 events in $\bar{p}+p \rightarrow \Lambda+\bar{\Lambda} +\pi^++\pi^-$ final states. The bands correspond to $Y_1^*(1385)$, i.e., $1350 \leqslant M(\Lambda\pi) \leqslant 1420$ MeV.

Production of Y_1^{*+} (and c.c.) and Y_1^{*-} (and c.c.) is particularly interesting because their ratio has some bearing on the single-particle exchange models. If single-particle exchange dominates in their production, Y_1^{*+} pair production should be favored over Y_1^{*-} pair production since the latter involves exchange of a doubly charged system. For the same reason, $Y_1^{*+}\bar{\Lambda}\pi^-$ (and c.c.) production should be favored over $Y_1^{*-}\bar{\Lambda}\pi^+$ (and c.c.). However, results from lower beam momenta do not agree with this expectation. For instance, data at 3.7 BeV/c [12] shows that there are at least as many $Y_1^{*-}(1385)$ pair events as $Y_1^{*+}(1385)$ events. Also $Y_1^{*-}(1385)$ production was found to be even stronger than that of $Y_1^{*+}(1385)$. This seeming contradiction may be related to the fact that the center-of-mass energy available at 3.7 BeV/c was only 130 MeV above the threshold of $Y_1^*(1385)$ pair production. Therefore single-particle exchange might not be expected to dominate. In this experiment, the energy available in the c.m. system is 3.86 BeV, much above the threshold of $\Lambda\bar{\Lambda}\pi^+\pi^-$ production. The angular distributions of the $\Lambda\pi^+$ (and c.c.) system and the $\Lambda\pi^-$ (and c.c.) system (Fig. 13) show that they were both produced very peripherally and that Y_1^{*-} and $\bar{Y}_1^{*+}$ were not produced as peripherally as Y_1^{*+} and $\bar{Y}_1^{*-}$. The histograms of the $\Lambda\pi$ systems (Fig. 14) show that Y_1^{*+} (and c.c.) production is much stronger than Y_1^{*+} (and c.c.) production. These are all consistent with single particle exchange models. It is clear from the scattergrams of the effective masses of the $\Lambda\pi$ systems (Fig. 15) that there was very little pair production of $Y_1^*(1385)$. This is in agreement with the general tendency for two-body production to become weaker at higher energies.

In the effective-mass distributions of both $\Lambda\pi^+$ (and c.c.) and $\Lambda\pi^-$ (and c.c.), there is a sharp enhancement

at a mass of 1630 MeV [Fig. 14(c)]. There are 16 combinations with mass between 1620 and 1640 MeV while phase space predicts four combinations after events with $Y_1^*(1385)$ have been subtracted. This enhancement, in any case, has $T=1$. At present, no Y_1^* resonance has been reported at this mass. However, with the low statistics available in this experiment we cannot determine whether this is a resonance or a statistical fluctuation.

VIII. SUMMARY

We found that the total hyperon production cross section in $\bar{p}$-p collisions at 6.935 BeV/c is 1.3 ± 0.1 mb, which is almost double that at 3.7 BeV/c. As the beam momentum increases from 3.7 to 7 BeV/c, cross sections for 2-body final states decrease, while cross sections for those final states with three or more particles greatly increase.

Although the energy available in the center-of-mass system is as large as 3.86 BeV, the study of all possible mass combinations of all final states did not yield statistically significant evidence for any new particle or resonance. We found some $Y_1^*(1385)$ production in every final state containing a $\Lambda\pi$ combination. Production of $Y_0^*(1405)$ and $Y_0^*(1520)$ was also observed. About 40% of all unique hyperon events in 3- to 5-body final states were produced with one or more of these resonances.

Angular distributions of all the hyperons and antihyperons observed show that about 90% of the hyperon events were highly peripheral while about 10% of them were approximately isotropic in the $\bar{p}$-p center-of-mass system. The sharp forward-backward peaking in the angular distributions of two-body final states can be fitted to a dominant $K^*(888)$ exchange modified by the absorption into competing channels. However, the cross sections for these states are too small by about a factor of 2 as compared with predictions from this model. On the other hand, ratios among the cross sections of 2-body final states agree well with predictions from a SU_3 octet exchange model with a pure F-type coupling. Charge ratios of $Y^{*\pm}(1385)$ and $\Sigma^{\pm}$ in various 3- and 4-body final states also demonstrate features predicted by single particle exchange models.

ACKNOWLEDGMENTS